arXiv:quant-ph/9701010v1 9 Jan 1997

Systematic and statistical errors in homodyne measurements of the density matrix

G. M. D'Ariano[a], C. Macchiavello[b], and N. Sterpi[a]

[a] *Dipartimento di Fisica 'A. Volta', Università degli Studi di Pavia via A. Bassi 6, I-27100 Pavia, Italy*

[b] *Clarendon Laboratory, University of Oxford Parks Road, OX1 3PU, Oxford, UK*

February 9, 2008

Abstract

We study both systematic and statistical errors in radiation density matrix measurements. First we estimate the minimum number of scanning phases needed to reduce systematic errors below a fixed threshold. Then, we calculate the statistical errors, intrinsic in the procedure that gives the density matrix. We present a detailed study of such errors versus the detectors quantum efficiency η and the matrix indexes in the number representation, for different radiation states. For unit quantum efficiency, and for both coherent and squeezed states, the statistical errors of the diagonal matrix elements saturate for large n. On the contrary, off-diagonal errors increase with the distance from the diagonal. For non unit quantum efficiency the statistical errors along the diagonal do not saturate, and increase dramatically versus both $1-\eta$ and the matrix indexes.

1 Introduction

The possibility of investigating quantum radiation states by homodyne detection techniques recently raised much interest[1]. In particular, progress has been made on the determination of an exact method to detect the density matrix directly from homodyne measurements, in any representation,

without resorting to any smoothing or filtering procedure of experimental data[2, 3, 4]. Such method can be basically summarized as follows. By means of homodyne detection, the field quadrature $\hat{x}_\phi = (a^\dagger e^{i\phi} + a e^{-i\phi})/2$ is measured at any desired phase shift ϕ with respect to the local oscillator ($a^\dagger$ and a are the creation and annihilation operators of the field mode). Then, the density matrix elements are obtained by averaging functions, called "kernel functions" (or "pattern functions"), on experimental data. We call this procedure "homodyning the density matrix" [5], to distinguish it from the previously used methods, where the density matrix was reconstructed after evaluating the Wigner function as an intermediate step (the celebrated "quantum tomography" [6, 7, 8]). The present method takes into account the detectors quantum efficiency, which must be greater than 0.5 for measuring the density matrix in the number representation[3].

In this paper, we numerically evaluate the measurement accuracy and the statistical errors in homodyning the density matrix, for both unit and non unit detectors quantum efficiency η. In Section 2 we briefly recall the direct method of homodyning the density matrix. Since each matrix element is given by an integral over scanning phases, whose number is necessarily finite, non negligible systematic errors arise if the number of phases is not large enough. Thus, in Section 3 we numerically estimate a lower value f_0 for the number of phases f, needed for an accurate measurement of a state, and we study the dependence of f_0 on the kind of state. We also investigate the convergence of the reconstructed matrix elements towards their respective theoretical values as functions of f. In Section 4 we introduce the statistical errors of the measured matrix elements. We study the errors as functions of the matrix indexes and of the quantum efficiency, for both coherent and squeezed states. We show that, for $\eta = 1$, the statistical errors of the diagonal matrix elements saturate for large n. This result is also analytically obtained after introducing an asymptotic approximation for the kernel functions. The off-diagonal errors increase with the distance from the diagonal. For $0.5 < \eta < 1$, we show that the statistical errors along the diagonal do not saturate, and increase dramatically versus both $1 - \eta$ and the matrix indexes. Due to such statistical errors, it is not convenient to use the measured density matrix elements to evaluate the expectation values of generic observables. Therefore, in the end of Section 4 we consider the possibility of *homodyning the observable*, i.e. measuring directly the expectation value of an observable by experimentally sampling an appropriate kernel function. In particular, we

consider the number of photons, and we calculate the precision of this kind of measurement. In Section 5 we conclude the paper, and in Appendix we report some useful calculations in detail.

2 Homodyning the density matrix

We briefly recall the method for homodyning the radiation density matrix $\hat{\rho}$. Our starting point is the operator identity[3]

$$\hat{\rho} = \int_0^{\pi} \frac{\mathrm{d}\phi}{\pi} \int_{-\infty}^{+\infty} \mathrm{d}k \, \frac{|k|}{4} \, \mathrm{Tr}[\hat{\rho} e^{ik\hat{x}_\phi}] \, e^{-ik\hat{x}_\phi} \,, \tag{1}$$

where the field quadrature is defined as $\hat{x}_\phi = (a^\dagger e^{i\phi} + a e^{-i\phi})/2$ and ϕ is the phase with respect to the local oscillator. The trace in Eq.(1) can be written in terms of quadrature probability distributions $p_\eta(x, \phi)$ at phase ϕ: for detectors quantum efficiency $\eta < 1$, such distributions are related to the ideal one ($\eta = 1$) by a Gaussian convolution so that in terms of characteristic functions one has

$$\mathrm{Tr}[\hat{\rho} e^{ik\hat{x}_\phi}] = e^{\frac{1-\eta}{8\eta}k^2} \int_{-\infty}^{+\infty} \mathrm{d}x \, p_\eta(x, \phi) \, e^{ikx} \,. \tag{2}$$

After exchanging integrals over k and x, Eq.(1) reads

$$\hat{\rho} = \int_0^{\pi} \frac{\mathrm{d}\phi}{\pi} \int_{-\infty}^{+\infty} \mathrm{d}x \, p_\eta(x, \phi) \, \hat{K}_\phi^{(\eta)}(x) \,. \tag{3}$$

In Equation (3), the kernel operator $\hat{K}_\phi^{(\eta)}(x)$ is

$$\hat{K}_\phi^{(\eta)}(x) = e^{i\phi a^\dagger a} \hat{\nu}^{(\eta)}(x) e^{-i\phi a^\dagger a} \tag{4}$$

with

$$\hat{\nu}^{(\eta)}(x) = \int_{-\infty}^{+\infty} \mathrm{d}k \frac{|k|}{4} \, e^{-\frac{2\eta-1}{8\eta}k^2 + ikx} \, : e^{-ik\frac{a^\dagger + a}{2}} : \tag{5}$$

(where $::$ denotes normal ordering). The operator $\hat{\nu}^{(\eta)}(x)$ can also be written as

$$\hat{\nu}^{(\eta)}(x) = \partial_x \hat{\mu}^{(\eta)}(x) \,, \tag{6}$$

with

$$\hat{\mu}^{(\eta)}(x) = \sqrt{2}\chi : e^{-\frac{a^\dagger + a}{2}\partial_x} : e^{-2\chi^2 x^2} \int_0^{\sqrt{2}\chi x} \mathrm{d}t\, e^{t^2} \tag{7}$$

and $\chi = \sqrt{\eta/(2\eta - 1)}$. Notice that, equivalently, one has

$$\hat{\mu}^{(\eta)}(x) = \sqrt{2}\chi e^{-\frac{a^\dagger + a}{2}\partial_x} e^{-\frac{1}{8}\partial_x^2} e^{-2\chi^2 x^2} \int_0^{\sqrt{2}\chi x} \mathrm{d}t\, e^{t^2}\,, \tag{8}$$

where the antidiffusion operator $\exp(-\partial_x^2/8)$ is due to normal ordering in Eq.(7).

The matrix elements $\rho(n,m) = \langle n|\hat{\rho}|m\rangle$ are evaluated by averaging the kernel functions [i.e. the matrix elements of the kernel operator $\hat{K}_\phi^{(\eta)}(x)$] calculated for random homodyne outcomes. As the experimental data are distributed according to the probability $p_\eta(x,\phi)$, such average gives a measurement of the density matrix. In other words, the density matrix is measured by experimentally sampling the kernel functions.

The kernel functions for homodyning the density matrix are reported in the following. We have carried out our analysis in the number representation, for η greater than the lower bound 0.5 (it has been shown that $\eta = 0.5$ is a universal lower bound for any representation[5]).

2.1 Unit quantum efficiency

For $\eta = 1$, Eq. (7) reads:

$$\hat{\mu}(x) = \sqrt{2} : e^{-\frac{a^\dagger + a}{2}\partial_x} : e^{-2x^2} \int_0^{\sqrt{2}x} \mathrm{d}t\, e^{t^2} \tag{9}$$

A simple and fast algorithm can be derived after writing the matrix elements $\langle n|\hat{\mu}(x)|m\rangle$ in factorized form. This technique was first introduced by Richter[9] for diagonal matrix elements, and was later generalized to off-diagonal matrix elements by Leonhardt *et al.*[10]. In Appendix we present a simple and alternative derivation which, in our opinion, is useful for further developments. The kernel functions are calculated from Eq.(32) and they read

$$\begin{aligned} \langle m+d|\hat{K}_\phi^{(\eta)}(x)|m\rangle &= e^{id\phi}\Big[4x\, u_m(x)v_{m+d}(x) - 2\sqrt{m+1}\, u_{m+1}(x)v_{m+d}(x) \\ &- 2\sqrt{m+d+1}\, u_m(x)v_{m+d+1}(x)\Big]\,, \end{aligned} \tag{10}$$

where the functions $u_j(x)$ and $v_j(x)$ are respectively the normalizable and the non normalizable eigenfunctions of the harmonic oscillator (corresponding to eigenvalue j).

2.2 Non unit quantum efficiency

For $\eta < 1$, no factorization algorithm is known at present. In this case, from Eq.(5) we obtain the following form for the kernel functions[3]:

$$\langle m+d|\hat{K}_{\phi}^{(\eta)}(x)|m\rangle = e^{id\phi} 2\chi^{d+2}\sqrt{\frac{m!}{(m+d)!}}e^{-\chi^2 x^2} \tag{11}$$
$$\times \sum_{\nu=0}^{m} \frac{(-)^{\nu}}{\nu!}\begin{pmatrix} m+d \\ m-\nu \end{pmatrix}(2\nu+d+1)!\chi^{2\nu}\mathrm{Re}\left\{(-i)^d D_{-(2\nu+d+2)}(-2i\chi x)\right\} ,$$

where $D_j(\sigma)$ denotes the parabolic cylinder function.

3 Systematic errors

In Equation (3) the density matrix is given by an integral over the phase ϕ with respect to the local oscillator. In order to avoid any systematic error, one should homodyne the density matrix at perfectly random phases. This is the case of the experimental method of Munroe *et al.*[13], where the photon number probability distribution is measured by homodyne detection: in such measurement no knowledge of the phase is needed, because the diagonal kernel functions are independent of ϕ. However, for measuring off-diagonal matrix elements the knowledge of the random phase is essential, and it is difficult to achieve. In such situation, the phase integral is usually performed by a phase scanning, as in Ref.[7]. An insufficient number of phases generates systematic errors, leading to values for the density matrix elements that are far from the true values. Therefore, in the experimental determination of the density matrix one has to eliminate these systematic errors as the first step.

The criterion adopted here to establish the degree of accuracy in a measurement is based on the *absolute* deviation of the measured matrix elements from the "true" matrix elements. For each $\rho(n,m)$, obtained from Eq.(3), we calculate the absolute deviation

$$\epsilon(n,m) = |\rho(n,m) - \rho_t(n,m)| , \tag{12}$$

where $\rho_t(n,m)$ is the true (theoretical) density matrix. For fixed state, the set $\{\epsilon(n,m)\}$ $(n,m=0,1,...)$ depends on the number of scanning phases f used in the experiment (the number of experimental data per scanning phase is kept fixed). We have an accurate matrix measurement when the maximum deviation is reduced below a fixed threshold, for example

$$\epsilon = \max_{n,m}\{\epsilon(n,m)\} < 10^{-4} \qquad (n,m=0,1...)\,. \tag{13}$$

Now, let us show how the accuracy depends on f for different radiation states.

The measurement accuracy increases with f. We expect that the more a radiation state is either displaced or "asymmetrically" distributed in phase space, the higher the number f must be. This is indeed the case. In Fig.1 we show the minimum number of phases f_0 needed for an accurate measurement of coherent and squeezed states. This number increases with both the average number of photons $\langle\hat{n}\rangle$ and the squeezing parameter r[12].

We point out that far off-diagonal kernel functions oscillate very fast as functions of ϕ, thus the larger the matrix dimension, the larger f_0. However, the main result, i.e. the increase of f_0 with $\langle\hat{n}\rangle$ and r, does not change. Indeed, both an increase and a decrease of the matrix dimension merely shift the plot in Fig.1 towards either higher or lower values of f_0. In the following we set $n_{max}=47$.

A comment about our choice for the accuracy criterion is now in order. Our purpose is to show the dependence of f_0 on the average energy and on the "asymmetry" in the phase space. This is achieved by calculating the absolute deviations $\{\epsilon(n,m)\}$: indeed, the systematic errors are independent of the size of the theoretical matrix element.

Finally, we briefly examine the dependence on the number of phases f for measurements of individual matrix elements.

We expect that for off-diagonal matrix elements the number of phases needed for an accurate measurement is larger than for diagonal ones, due to faster oscillations of the integrand in Eq.(3) versus ϕ. For coherent states this is generally true, as shown for example in Fig.2, where $\epsilon(5,5) < 10^{-4}$ for $f \geq 14$, and $\epsilon(18,5) < 10^{-4}$ for $f \geq 24$. For squeezed states the behavior on the distance from the diagonal is more complicated. In many cases the same result of coherent states is found, see for example Fig.3, where the diagonal element $\rho(5,5)$ converges faster than $\rho(10,5)$ and $\rho(15,5)$ for large enough f. However, there are exceptions to this behavior. As an example, in Fig.4

we show the asymptotically slower convergence of $\rho(10,10)$ with respect to $\rho(10,9)$ and $\rho(10,0)$.

4 Statistical errors

The statistical errors on the measured matrix elements are calculated in terms of the errors on real and imaginary parts of the matrix. For a matrix element $\rho(n,m)$ the real part of the statistical variance is defined as

$$\begin{aligned} \mathrm{Re}^2\{\sigma(n,m)\} &= \int_0^\pi \frac{\mathrm{d}\phi}{\pi} \int_{-\infty}^{+\infty} \mathrm{d}x\, p_\eta(x,\phi)\, \mathrm{Re}^2\{\langle n|\hat{K}_\phi^{(\eta)}(x)|m\rangle\} \\ &- \mathrm{Re}^2\{\rho(n,m)\} \end{aligned} \tag{14}$$

and analogously for the imaginary part. The experimental error of the measurement is obtained by rescaling the amplitudes $|\sigma(n,m)|$ by a factor $1/\sqrt{N}$, where N is the total number of experimental data. For simplicity, hereafter the quantity $\sigma(n,m)$ will be called statistical error. The statistical errors turn out to be independent of f if $f > f_0$. Thus, we focus attention on the general features of the set $\{\sigma(n,m)\}$ for different radiation states, at fixed f. First we show the results for unit quantum efficiency η, later we will consider the dependence on η.

4.1 General features for unit quantum efficiency

For coherent and squeezed radiation states, the real and imaginary parts of the statistical errors exhibit a similar behavior as functions of the matrix indexes (with the major exception of the matrix diagonal, where obviously $\mathrm{Im}\{\sigma(n,n)\} \equiv 0$). Thus, without loss of generality, we can show our results in terms of the amplitudes $|\sigma(n,m)|$.

In Fig.5 we report the matrix of errors $|\sigma(n,m)|$ for a coherent state with $\langle\hat{n}\rangle = 4$. The contour plot shows that errors increase with the distance $d = n - m$ from the diagonal. This is related to the analytical form of the kernel operator. In particular, for fixed ϕ, all the kernel functions are oscillating functions of x[14]. Moreover, for increasing d the oscillations become faster and the oscillation range slowly increases. If a kernel function oscillates fast, its statistical average becomes more sensitive to fluctuations of experimental data and, therefore, the statistical errors must increase versus d.

The contour plot also emphasizes the "saddle region" around the diagonal, suggesting that the statistical errors for measured diagonal matrix elements saturate to a value independent of n for large enough n. This is shown more clearly in Fig.6. Such a remarkable feature is general. In fact, it is independent on the energy $\langle \hat{n} \rangle$ and, more important, it holds for any state. Noticeably, the limiting value $|\sigma(n,n)| = \sqrt{2}$ does not depend the degree of squeezing. The reason for such saturation is due to the analytic form of the diagonal kernel functions. Indeed, the larger n is, the faster the kernel functions oscillate vs. x and the errors must increase with n. On the other hand, for $d = 0$ the range of oscillation is fixed between -2 and 2, thus the diagonal errors are bounded, and hence they must saturate. These considerations are confirmed by considering the explicit form of the statistical errors, as given by Eq.(14). In particular, from Eq.(14) we can extract the relevant contribution for large n upon considering that the kernel functions oscillate fast in the region where $p(x,\phi)$ is sizeable. Moreover, $p(x,\phi)$ has a Gaussian decay, whereas the kernel functions decrease as a power of x. Thus,

$$|\sigma(n,n)| \simeq \left\{ \int_0^{\pi} \frac{\mathrm{d}\phi}{\pi} \int_{-\infty}^{+\infty} \mathrm{d}x \, p(x,\phi) \, 4\cos^2(k_n x) \right\}^{1/2} . \tag{15}$$

For large values of n, $k_n \to \infty$: if $p(x,\phi)$ can be considered constant over a cycle $\Delta x = \pi/k_n$, the integral over x in Eq. (15) gives just the average of $\cos^2(k_n x)$, which leads to

$$|\sigma(n,n)| \simeq \sqrt{2} \, . \tag{16}$$

If very squeezed states are considered [i.e. with very sharp $p(x,\phi)$] the errors will saturate for larger n. In Fig.7 we show $|\sigma(n,m)|$ for a squeezed state with $\langle \hat{n} \rangle = 4$ and $r = 1$: the plot is quite different from Fig.5, but the diagonal errors still saturate.

4.2 Dependence on the quantum efficiency

The influence of the quantum efficiency η on $|\sigma(n,m)|$ is very strong. Indeed, for non unit quantum efficiency of detectors the behavior of the kernel functions (12) changes dramatically: for fixed n and m, the oscillation range increases very rapidly as η approaches the lower bound $\eta = 0.5$, and the

resulting errors increase rapidly as well. The growth rate is different for different matrix elements: as an example, in Fig.8 we show some diagonal errors as functions of quantum efficiency (for a coherent state). Furthermore, the diagonal errors no longer saturate for large values of n. Very similar results are found for squeezed states. In particular, the growth rate of diagonal errors $|\sigma(n,n)|$ vs. $1-\eta$ is slightly larger than for coherent states. The diagonal errors for a squeezed state are shown in Fig.9 for different values of η.

For fixed $\eta < 1$, the oscillation range of the kernel functions increases with both n and the distance d from the diagonal. Thus, for increasing n and d the statistical errors increase. For example, we consider $\eta = 0.99$: after a comparison between Fig.10 and Fig.5, one can see that the open contour levels for $|\sigma(n,m)|$ close, and any errors saturation disappears. Figure 10 shows that drastic modifications arise with respect to the ideal case for $\eta = 1$. This means that, already for $\eta = 0.99$, in order to have the same experimental errors on the measurement of the density matrix, the number of data must be much larger than in the ideal case.

4.3 Precision of homodyning observables

From the measured density matrix, one can evaluate the probability distributions of operators that are functions of the field operators a and $a^\dagger$. Thus, by means of homodyne experimental data it is possible to obtain indirect measurements of observables. However, for some observables the propagation law of statistical errors leads to additional noise with respect to direct detection. In some cases, such indirect detection through the density matrix can be overcome by a more convenient procedure, namely *homodyning the observable*. By *homodyning the observable* we mean the experimental sampling of an appropriate kernel function, which directly gives the expectation value of the desired observable.

We consider, as an example, the homodyne measurement of the mean photon number $\langle \hat{n} \rangle$. From Eq.(1), $\langle \hat{n} \rangle$ is expressed as

$$\langle \hat{n} \rangle = \int_0^\pi \frac{\mathrm{d}\phi}{\pi} \int_{-\infty}^{+\infty} \mathrm{d}x \, p(x,\phi) \, F(x,\phi) \tag{17}$$

where

$$F(x,\phi) \equiv F(x) = \sum_{n=0}^{\infty} n \int_{-\infty}^{+\infty} \mathrm{d}k \, \frac{|k|}{4} \, e^{-\frac{1}{8}k^2 + ikx} \, L_n^{(0)}\left(\frac{k^2}{4}\right) = 2x^2 - \frac{1}{2} \, . \tag{18}$$

In Equation (18), $L_n^{(0)}$ denote zero-order Laguerre polynomials and unit detectors efficiency has been considered. The statistical fluctuations of the measured mean photon number are given by

$$\sigma^2_{\langle\hat{n}\rangle} = \int_0^\pi \frac{\mathrm{d}\phi}{\pi} \int_{-\infty}^{+\infty} \mathrm{d}x\, p(x,\phi)\, F^2(x,\phi) - \langle\hat{n}\rangle^2 \,. \tag{19}$$

and $\sigma_{\langle\hat{n}\rangle}$ is the statistical error for homodyning the mean photon number. The precision $\epsilon_{\langle\hat{n}\rangle}$ of this homodyne measurement is defined by the relation

$$\epsilon^2_{\langle\hat{n}\rangle} = \sigma^2_{\langle\hat{n}\rangle} - \langle\Delta\hat{n}^2\rangle \,, \tag{20}$$

where $\langle\Delta\hat{n}^2\rangle$ is the intrinsic quantum uncertainty

$$\langle\Delta\hat{n}^2\rangle \;\equiv\; \langle\hat{n}^2\rangle - \langle\hat{n}\rangle^2 = \langle a^{\dagger 2} a^2\rangle + \langle\hat{n}\rangle - \langle\hat{n}\rangle^2 \,. \tag{21}$$

The uncertainty $\langle\Delta\hat{n}^2\rangle$ can be expressed in terms of quadrature probability distributions: after calculating the kernel function for operator $a^{\dagger 2}a^2$[15], Eq.(21) reads

$$\langle\Delta\hat{n}^2\rangle = \int_0^\pi \frac{\mathrm{d}\phi}{\pi} \int_{-\infty}^{+\infty} \mathrm{d}x\, p(x,\phi) \left\{ \frac{8}{3}x^4 - 2x^2 \right\} - \langle\hat{n}\rangle^2 \,. \tag{22}$$

In conclusion, the precision for homodyning the photon number is

$$\epsilon_{\langle\hat{n}\rangle} = \frac{1}{\sqrt{2}} \left(\langle\Delta\hat{n}^2\rangle + \langle\hat{n}\rangle^2 + \langle\hat{n}\rangle + 1 \right)^{1/2} \,. \tag{23}$$

5 Conclusions

We analyzed both systematic and statistical errors for homodyne detection of the density matrix of light. Such detection is performed by suitably processing homodyne experimental data. We studied the behavior of systematic errors as functions of the number of scanning phases f. We calculated the lower bound for f, needed for an accurate matrix measurement. We found that this lower bound increases with both the mean photon number and the "asymmetry" in phase space of the state. Then we considered the statistical errors corresponding to the data average that gives each matrix element. Noticeably, for unit quantum efficiency of the detectors the diagonal errors

$\sigma(n,n)$ of the matrix elements $\rho(n,n)$ "saturate" to the fixed value $\sqrt{2}$ for large enough n. This feature is independent of the degree of squeezing. The off-diagonal errors increase with the distance from the diagonal. If detectors quantum efficiency is decreased, the errors increase for each matrix element. In particular, any saturation effects disappear. Finally, we considered the homodyne detection of the mean photon number, that is achieved by sampling an appropriate kernel function, and we analytically evaluated the precision of such measurement. We think that the results presented here are relevant from a fundamental point of view and provide the experimentalist with important information on the behavior of errors in homodyning the density matrix.

6 Appendix

The factorization of the matrix element $\langle m+d|\hat{\mu}(x)|m\rangle$ is performed in two steps. By setting $n = m + d$ we obtain

$$\begin{aligned}\langle m+d|\hat{\mu}(x)|m\rangle &= \sqrt{\frac{m!}{(m+d)!}}\sum_{\nu=0}^{m}\left(\begin{array}{c} m+d \\ \nu+d \end{array}\right)\frac{1}{\nu!} \\ &\times \left(-\frac{\partial_x}{2}\right)^{2\nu+d}\sqrt{2}e^{-2x^2}\int_0^{\sqrt{2}x}\mathrm{d}t\, e^{t^2}\,. \end{aligned} \tag{24}$$

Then, the derivatives with respect to x and the summation are evaluated as follows. We introduce the "seed functions"

$$u_0(x) = \left(\frac{2}{\pi}\right)^{1/4} e^{-x^2} \tag{25}$$

$$v_0(x) = (2\pi)^{1/4}\, e^{-x^2}\int_0^{\sqrt{2}x}\mathrm{d}t\, e^{t^2} \tag{26}$$

that generate two sets of functions $\{u_j(x)\}$ and $\{v_j(x)\}$ for $j = 0, 1, 2...$, as

$$u_j(x) = \frac{1}{\sqrt{j!}}\left(x - \frac{\partial_x}{2}\right)^j u_0(x) \tag{27}$$

$$v_j(x) = \frac{1}{\sqrt{j!}}\left(x - \frac{\partial_x}{2}\right)^j v_0(x)\,. \tag{28}$$

By means of the following identity between operators

$$\partial_x u_0(x) = u_0(x)(\partial_x - 2x)\,, \tag{29}$$

we obtain

$$\left(-\frac{\partial_x}{2}\right)^d u_0(x)v_0(x) = \sqrt{d!}\, u_0(x)v_d(x)\,. \tag{30}$$

As noticed in Ref. [10], the functions $\{u_j(x)\}$ and $\{v_j(x)\}$ are respectively the normalizable and the non normalizable eigenfunctions of the harmonic oscillator (corresponding to eigenvalue j). Thus, by using the standard recursion relations for the harmonic oscillator eigenfunctions, we can easily demonstrate the following identity[11]:

$$\frac{1}{\nu!}\left(-\frac{\partial_x}{2}\right)^{2\nu} u_0(x)v_d(x) = \sum_{j=0}^{\nu}\sqrt{\left(\begin{array}{c} j+d \\ j \end{array}\right)}(-1)^{\nu-j}\left(\begin{array}{c} \nu+d \\ j+d \end{array}\right) u_j(x)v_{j+d}(x)\,. \tag{31}$$

After substituting (30) and (31) in Eq.(24), we obtain the factorized formula

$$\langle m+d|\hat{\mu}(x)|m\rangle = \langle m|\hat{\mu}(x)|m+d\rangle = u_m(x)v_{m+d}(x)\,, \tag{32}$$

where we use the fact that $\hat{\mu}(x)$ is real selfadjoint. Finally, the kernel functions are obtained using Eqs. (4),(6) and (32).

References

[*] E-mail: dariano@pv.infn.it

[1] A review on methods to measure quantum states of radiation is given by U. Leonhardt and H. Paul, Prog. Quantum Electron. **19**, 89 (1995).

[2] G.M. D'Ariano, C. Macchiavello, and M.G.A. Paris, Phys. Rev. A **50**, 4298 (1994).

[3] G.M. D'Ariano, U. Leonhardt, and H. Paul, Phys. Rev. A **52**, R1801 (1995).

[4] U. Leonhardt, H. Paul, and G.M. D'Ariano, Phys. Rev. A **52**, 4899 (1995).

[5] A recent review on both the new direct method for reconstructing the density matrix from homodyne data and the previous tomographic methods is given by G. M. D'Ariano, *Measuring quantum states*, in *Concepts and Advances in Quantum Optics and Spectroscopy of Solids*, ed. by T. Hakioglu and A.S. Shumovsky (Kluwer, Amsterdam, in press).

[6] K. Vogel and H. Risken, Phys. Rev. A **40**, 2847 (1989).

[7] D.T. Smithey, M. Beck, M.G. Raymer, and A. Faridani, Phys. Rev. Lett. **70**, 1244 (1993).

[8] H. Kühn, D.-G. Welsch, W. Vogel, J. Mod. Opt. **41**, 1607 (1994).

[9] Th. Richter, Phys. Lett. A **211**, 327 (1996).

[10] U. Leonhardt, M. Munroe, T. Kiss, Th. Richter, and M. G. Raymer, Opt. Comm. **127**, 144 (1996).

[11] Equation (31) is demonstrated by means of the recursion relation

$$\frac{\partial_x^2}{4} u_m(x) v_{m+d}(x) = \sqrt{m(m+d)}\, u_{m-1}(x) v_{m-1+d}(x)$$
$$- (1+2m+d)\, u_m(x) v_{m+d}(x) + \sqrt{(m+1)(m+1+d)}\, u_{m+1}(x) v_{m+1+d}(x)\,.$$

[12] For squeezing parameter r, one has $\langle \hat{n} \rangle - \sinh^2 r = |\langle a \rangle|^2$.

[13] M. Munroe, D. Boggavarapu, M. E. Anderson, and M. G. Raymer, Phys. Rev. A **52**, R924 (1995).

[14] G.M. D'Ariano, Quantum Semiclass. Opt. **7**, 693 (1995).

[15] Th. Richter, Phys. Rev. A **53**, 1197 (1996).

Figure 1: Minimum number of scanning phases f_0 required by the condition $\epsilon < 10^{-4}$ vs. the mean number of photons $\langle \hat{n} \rangle$ for coherent states (circles), squeezed states with $r = 0.6$ (triangles), and $r = 1$ (squares). [The matrix dimensions are fixed to $n_{max} = 47$.]

Figure 2: Absolute deviation $\epsilon(n, m)$ vs. f for a coherent state with $\langle \hat{n} \rangle = 4$: $(n, m) = (5, 5)$ (circles), $(n, m) = (10, 5)$ (triangles), $(n, m) = (18, 5)$ (squares). The theoretical matrix elements are $\rho_t(5, 5) = 0.15629$, $\rho_t(10, 5) = 0.02876$, $\rho_t(18, 5) = 0.00017$.

Figure 3: Absolute deviation $\epsilon(n, m)$ vs. f for a squeezed state with $\langle \hat{n} \rangle = 4$, $r = 1$: $(n, m) = (5, 5)$ (circles), $(n, m) = (10, 5)$ (triangles), $(n, m) = (15, 5)$ (squares). The theoretical matrix elements are $\rho_t(5, 5) = 0.04182$, $\rho_t(10, 5) = 0.03231$, $\rho_t(15, 5) = 0.01852$.

Figure 4: Absolute deviation $\epsilon(n, m)$ vs. f for a squeezed state with $\langle \hat{n} \rangle = 4$, $r = 1$: $(n, m) = (10, 10)$ (circles), $(n, m) = (10, 9)$ (triangles), $(n, m) = (10, 0)$ (squares). The theoretical matrix elements are $\rho_t(10, 10) = 0.02495$, $\rho_t(10, 9) = 0.02418$, $\rho_t(10, 0) = 0.09307$.

Figure 5: Statistical error amplitudes $|\sigma(n, m)|$ for a coherent state with $\langle \hat{n} \rangle = 4$ ($\eta = 1$).

Figure 6: $|\sigma(n, n)|$ for: coherent state with $\langle \hat{n} \rangle = 4$ (circles), squeezed state with $\langle \hat{n} \rangle = 4$, $r = 1$ (triangles) ($\eta = 1$).

Figure 7: $|\sigma(n, m)|$ for a squeezed state with $\langle \hat{n} \rangle = 4$, $r = 1$ ($\eta = 1$).

Figure 8: $|\sigma(n, n)|$ vs. $1 - \eta$ for $n = 0, 2, 5, 15$ on a semilogarithmic scale (for a coherent state with $\langle \hat{n} \rangle = 4$). The quantum efficiencies are $\eta = 1, 0.99, 0.97, 0.95, 0.9$.

Figure 9: $|\sigma(n,n)|$ for a squeezed state with $\langle\hat{n}\rangle = 4$, $r = 1$ for: $\eta = 1$ (circles), $\eta = 0.99$ (triangles), $\eta = 0.97$ (squares), $\eta = 0.95$ (rhombi), $\eta = 0.9$ (stars).

Figure 10: $|\sigma(n,m)|$ for a coherent state with $\langle\hat{n}\rangle = 4$ for quantum efficiency $\eta = 0.99$.

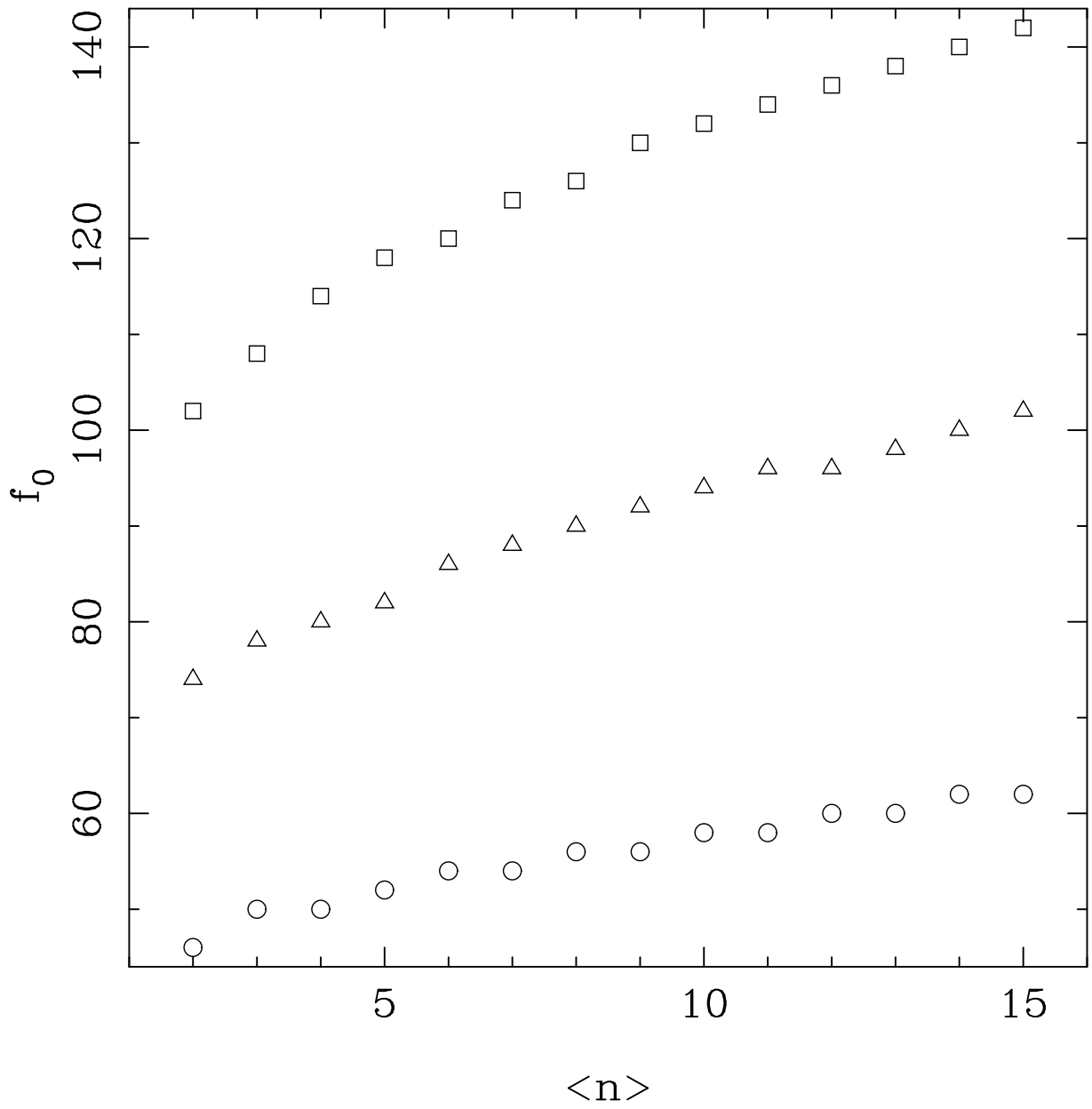

Fig.1 G.M. D'Ariano et al.

Systematic and statistical errors...

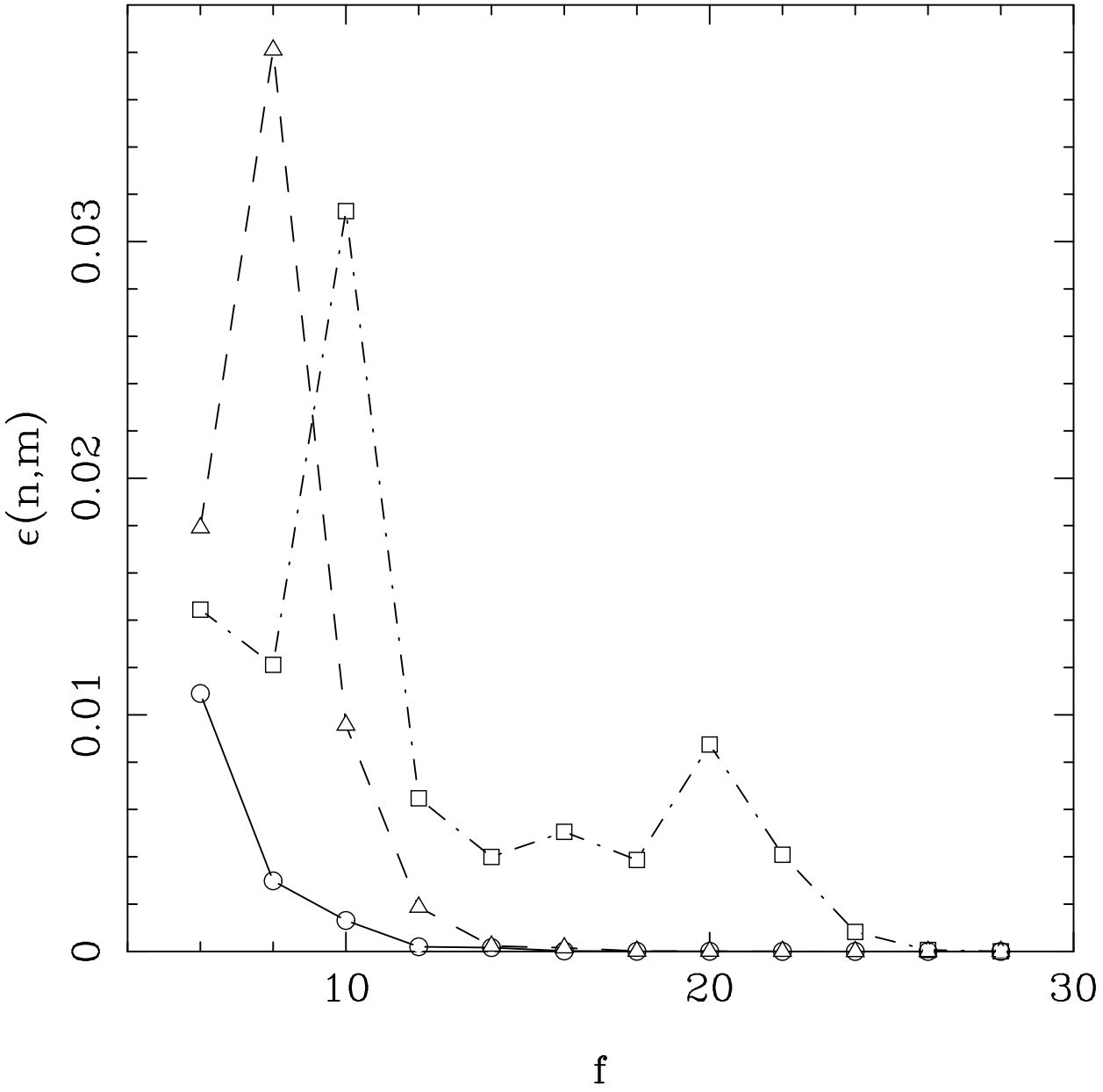

Fig.2 G.M. D'Ariano et al.

Systematic and statistical errors...

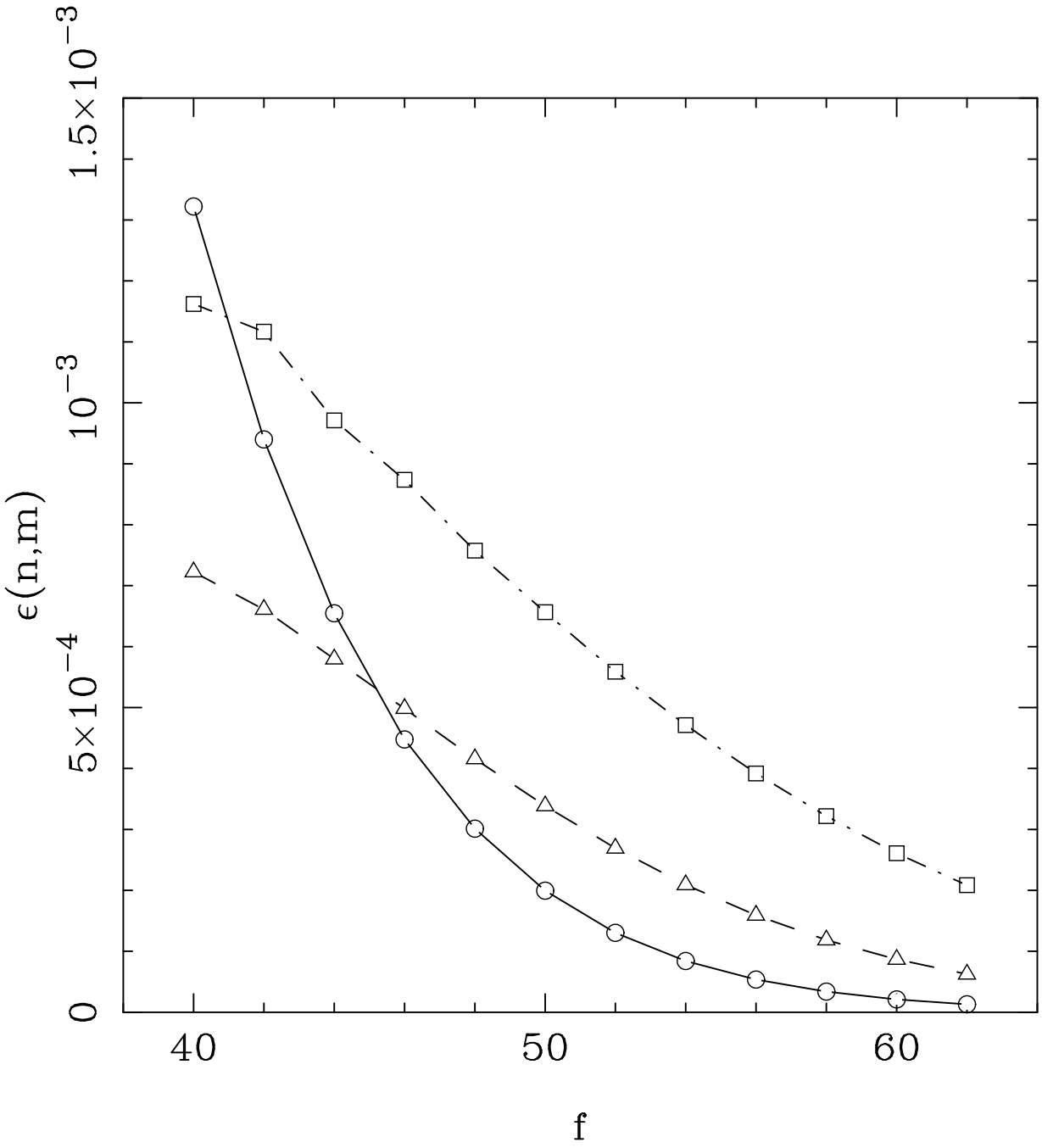

Fig.3 G.M. D'Ariano et al.

Systematic and statistical errors...

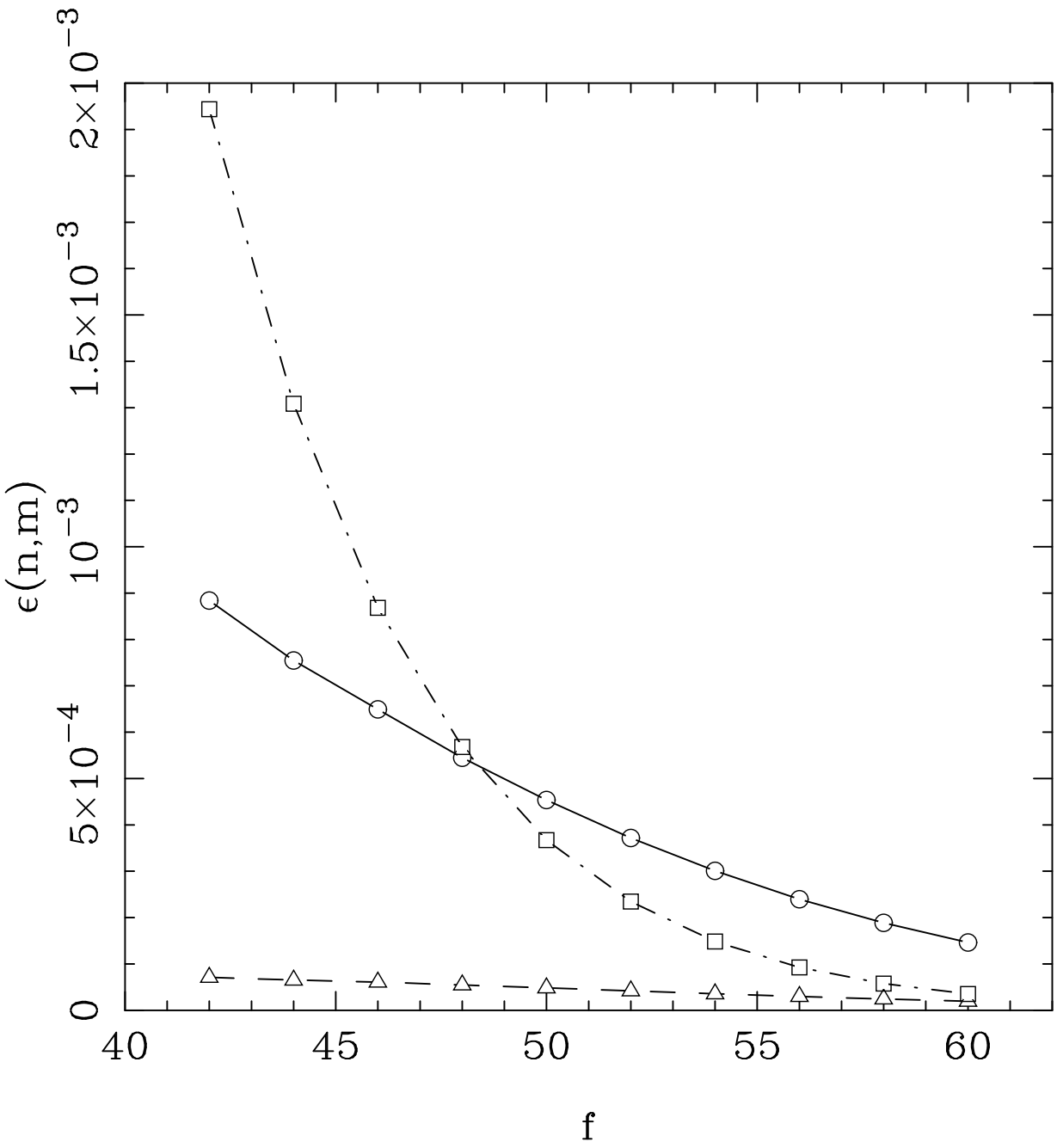

Fig.4 G.M. D'Ariano et al.

Systematic and statistical errors...

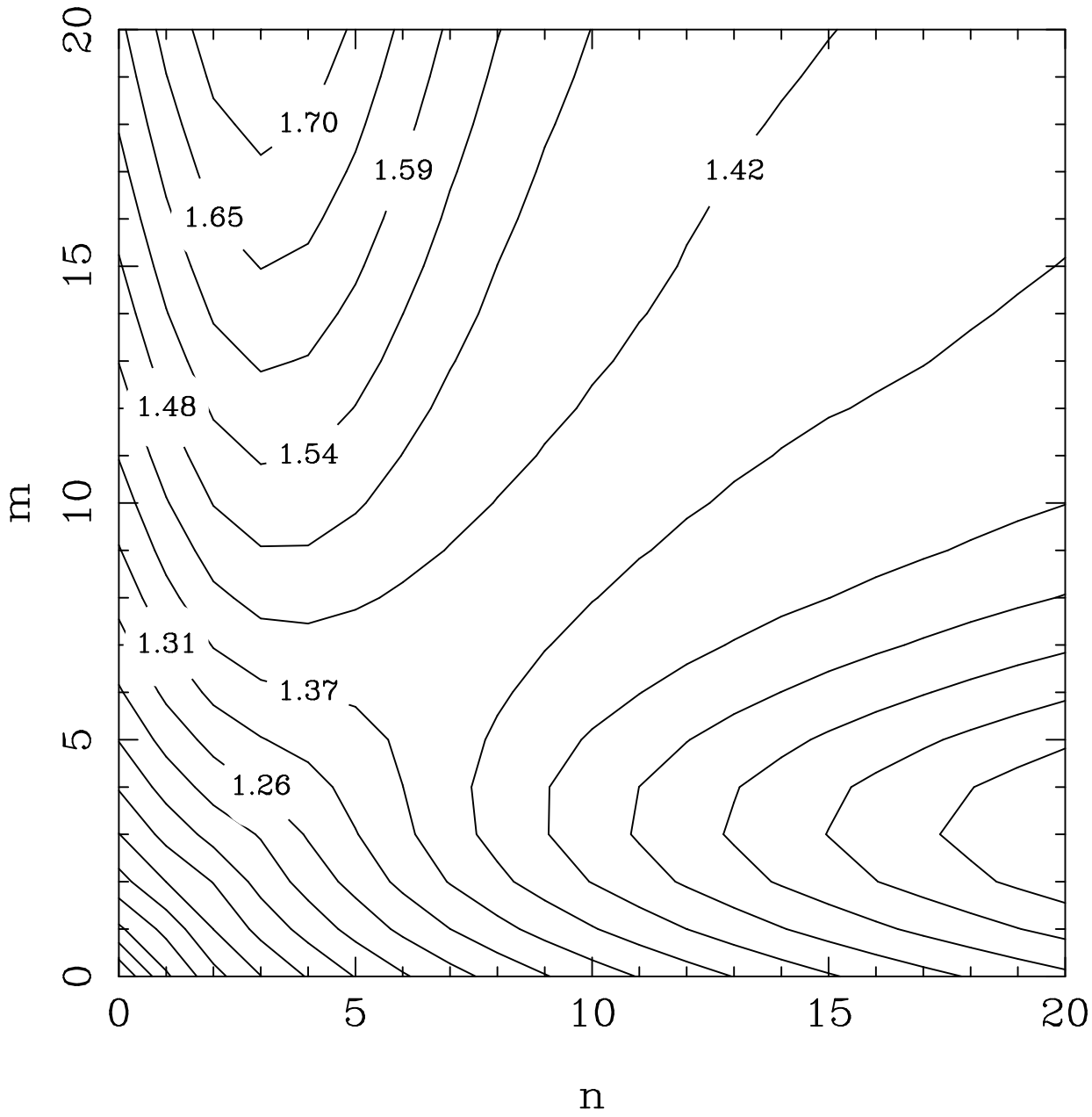

Fig.5 G.M. D'Ariano et al.

Systematic and statistical errors...

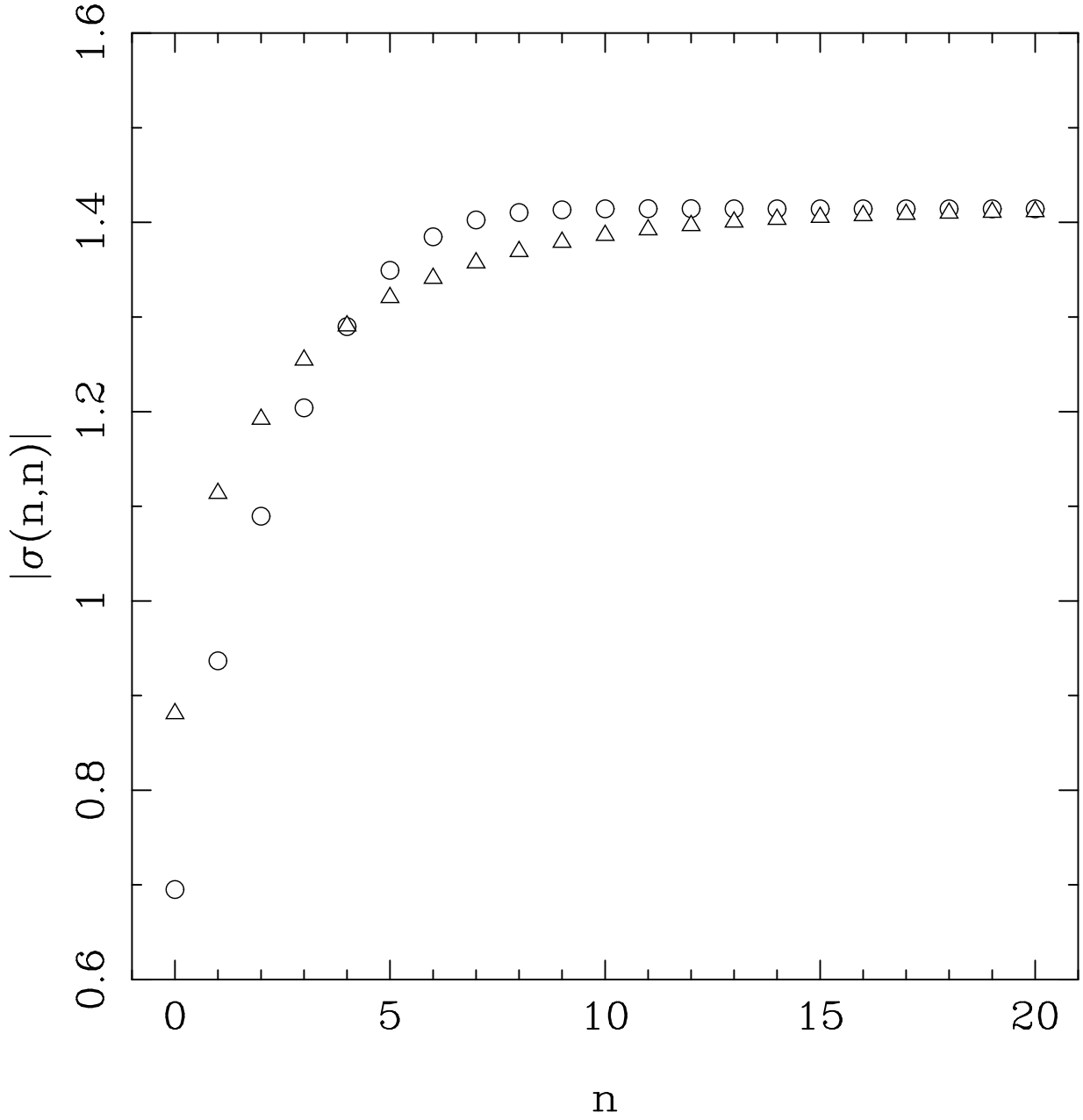

Fig.6 G.M. D'Ariano et al.

Systematic and statistical errors...

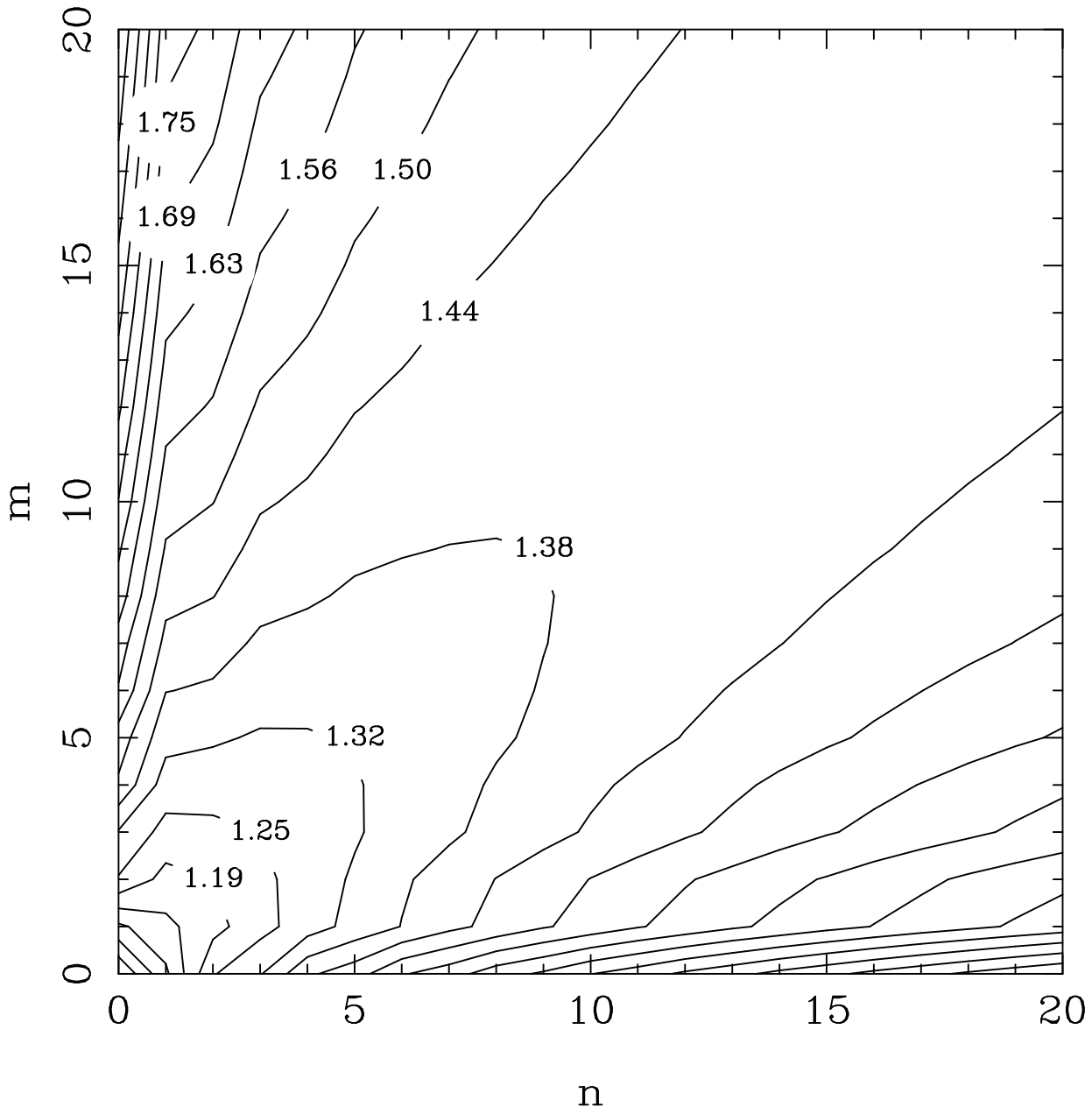

Fig.7 G.M. D'Ariano et al.

Systematic and statistical errors...

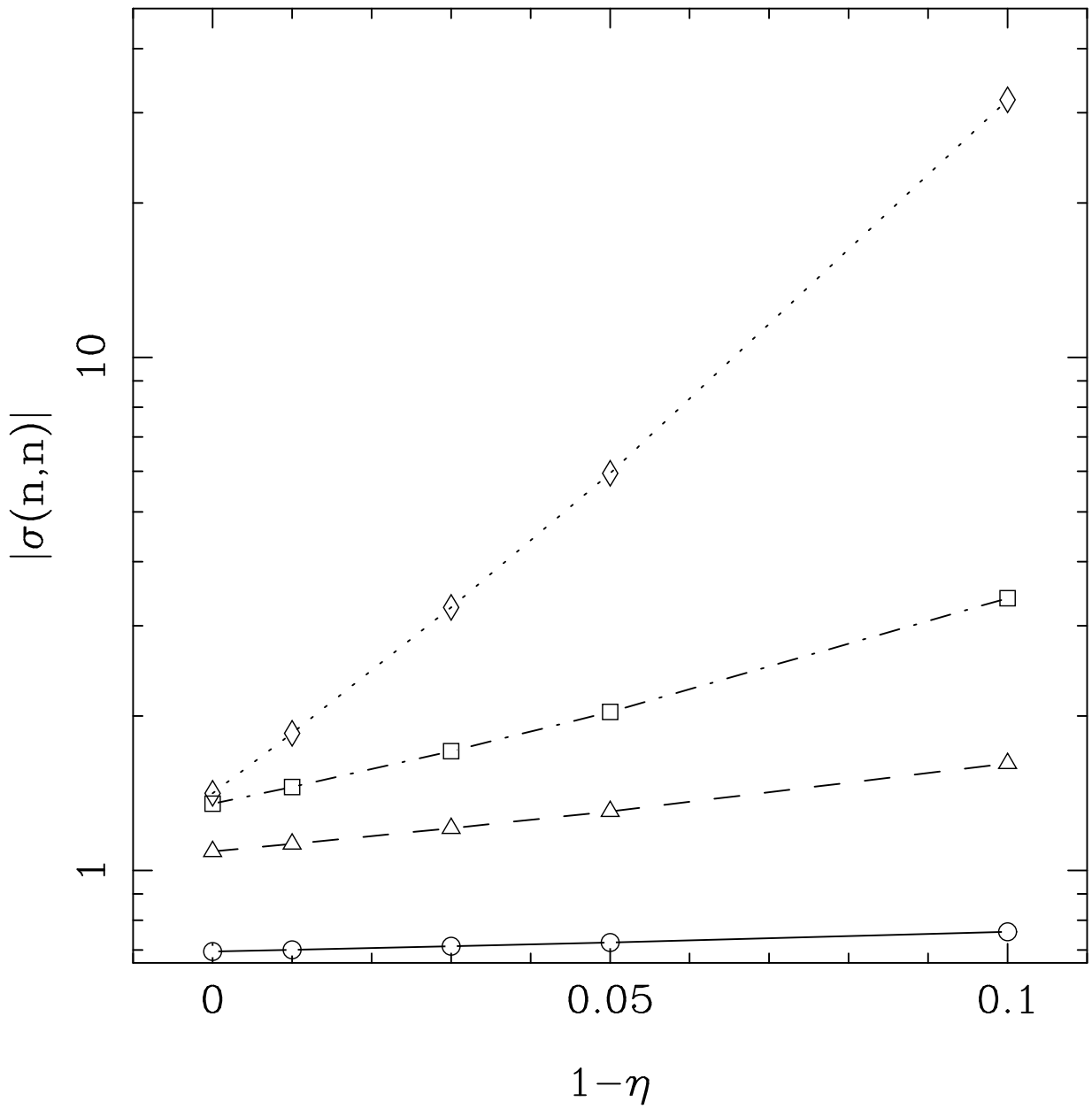

Fig.8 G.M. D'Ariano et al.

Systematic and statistical errors...

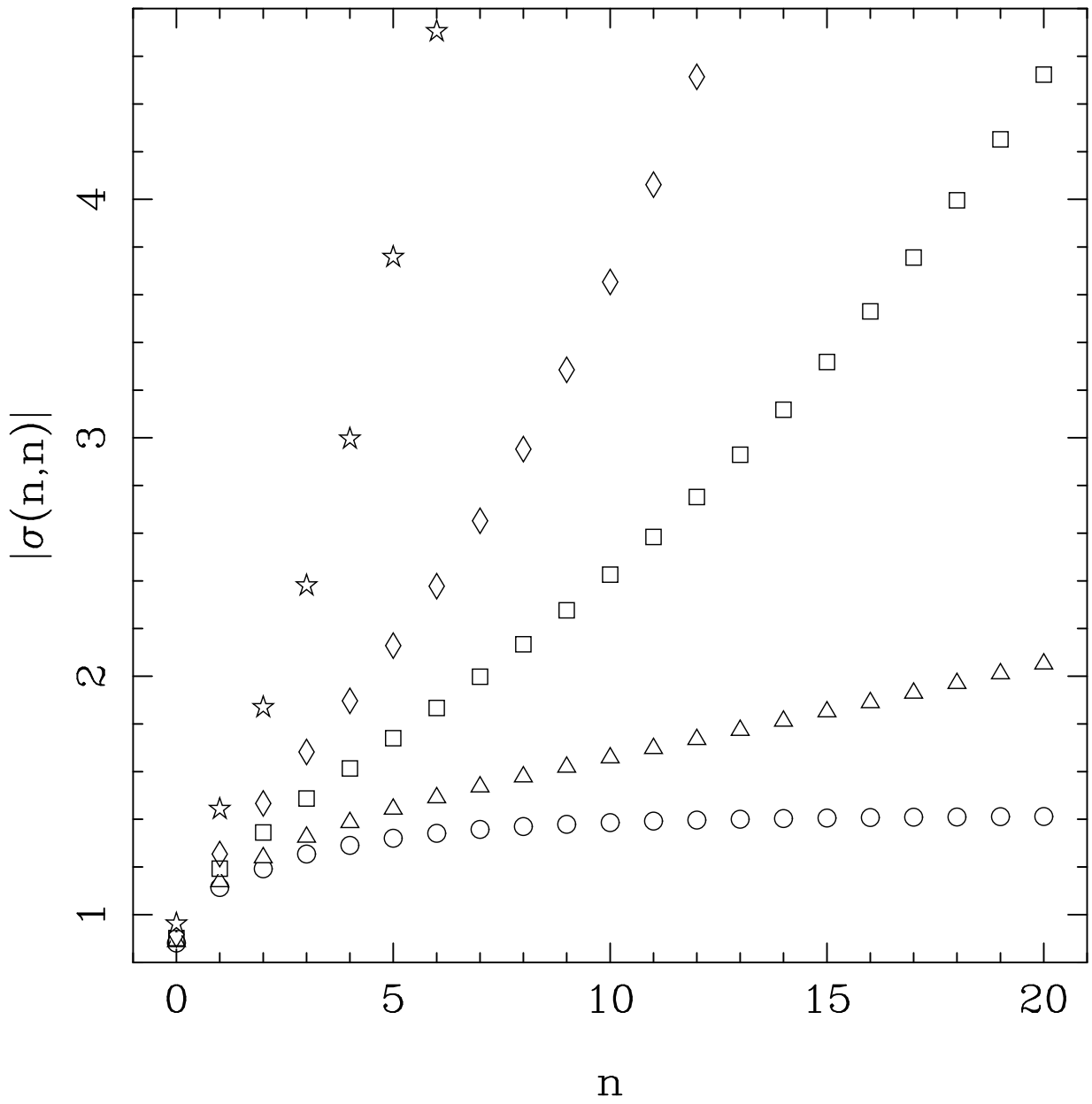

Fig.9 G.M. D'Ariano et al.

Systematic and statistical errors...